High-*Q* photonic crystal cavities with embedded quantum dots

K. Hennessy[*a], C. Reese[a], A. Badolato[a], A. Imamoğlu[a, b], P. M. Petroff[a, c], E. L. Hu[a, c]

[a]Department of Electrical and Computer Engineering
[b]Department of Physics
[c]Materials Department
University of California, Santa Barbara, CA 93106

ABSTRACT

Defects in photonic crystals (PCs) can support localized light modes with extremely small mode volumes. Depending on the symmetry of the PC, and the means of fabrication of the PC, extremely high quality factors (*Q*) are also possible. The combination of high *Q* and small mode volume should allow us to observe strong coupling between the cavity and quantum dot (QD) emitters that are strategically embedded within the cavity. This, in turn, has important implications for a variety of optical phenomena, such as single-photon sources. We describe the fabrication of PCs formed within membranes (180 nm thick) of GaAs, of either triangular or square lattice symmetry. The structures incorporate InAs QDs, grown monolithically with the PC material by Molecular Beam Epitaxy (MBE). We have observed emission from the smallest volume cavities (i.e. single-hole defects) in both the triangular and square lattice structures. The cavities have lattice constants ranging from 0.25 – 0.40 μm, and *Q* factors as high as 8500. To improve the probability of coupling a single QD to a cavity mode, we have developed a lithographic positioning technique capable of aligning a cavity to a feature on the surface within 50 nm, adequate to overlap a QD with a cavity mode. We will report on the progress achieved thus far with these structures and the challenges remaining to achieve strong coupling with specific QDs.

1. INTRODUCTION

Semiconductor quantum dots (QDs) exhibit discrete optical transitions with ultra-narrow (3.4 μeV at 2 K)[1] linewidths, making them well suited for use as an emitter in various nanoscale photonic devices. Due to their self-assembling method of formation, QDs have many advantages over other types of emitters such as neutral atoms or impurity levels. For example, their larger size allows QDs to be located by standard nanoscale metrological techniques, and by varying the growth conditions the QD emission spectrum can be continuously shifted. These properties make QDs well suited for integration in future quantum-optical devices as manageable and tunable emitters.

A QD may be 'functionalized' by positioning it in a nanoscale photonic cavity and engineering the strength of coupling between a discrete QD transition and an electromagnetic mode of the cavity. Various types of devices useful for quantum information processing may be realized in this way. A challenge to making useful devices is to design and construct a cavity that confines the optical field well and in a small volume, thus maximizing the strength of coupling with the QD. This amounts to fabricating a cavity that supports a mode of high quality factor *Q* and small volume *V*. The primary focus of our work is to demonstrate a cavity of high *Q/V*.

Cavities defined by defects in two-dimensional photonic crystals are relatively easy to fabricate and can support optical modes of very small *V*. In recent years the sources of loss in this class of devices has become well understood and cavities that also possess high *Q* have been predicted and experimentally realized[2-13]. With this combination of high *Q* and small *V*, planar photonic crystal nanocavities are very promising candidates for the observation of strong coupling with a single QD. We demonstrate that significant improvement in cavity *Q* can be achieved by first carefully considering the photonic crystal symmetry and defect type and then optimizing device fabrication. To illustrate this point, we compare cavities of various defect type in both triangular and square lattices and observe the sensitivity of their optical behavior to inadvertent variation in photonic crystal hole size and sidewall inclination.

[*] Electronic mail: *kjh@ece.ucsb.edu*

Strongly coupling a QD to a nanocavity entails precise spatial positioning of the QD at the electric field antinode of the cavity mode. In single-hole defect cavities, V is small enough to bring into question the feasibility of achieving this alignment probabilistically, simply by fabricating and testing a large number of cavities. We address this concern by developing and evaluating a lithographic alignment technique that actively positions a photonic crystal around a small feature of known distance from a metal alignment mark. Future work will focus on positioning our high Q/V cavities to specific QDs using this technique, creating functional devices for quantum information processing.

2. InAs/GaAs PARTIALLY COVERED ISLANDS

The self-assembly of semiconductor QDs from the Stranski-Krastanov growth mode has been widely studied within the last decade. The basic ideas which govern the growth dynamic of these heterostructures have been established and high quality, coherent nano-islands have been reported by several groups[14]. The capability of zero-dimensional devices to surpass higher-dimensional semiconductor structures in classical optoelectronic applications is still a matter of discussion, but extensive single-dot spectroscopy has yielded a broad agreement on the identification of QDs as artificial atoms[15] and useful as atom-like emitters in devices. With respect to real atoms, these islands of ~10 nm size can be spatially discriminated and therefore integrated into an optically or electrically addressing architecture. Through these prospects, self-assembled QDs can be the material of choice for experimental implementations of quantum information processing[16].

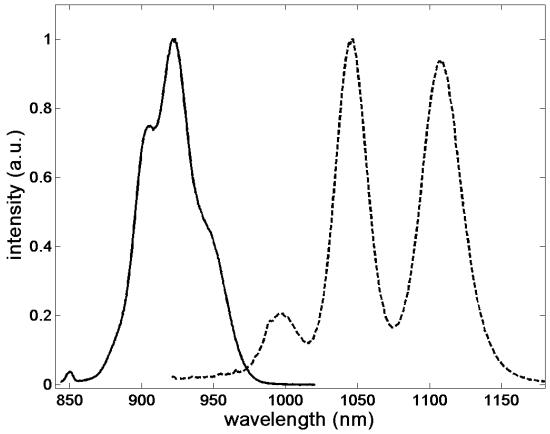

Fig. 1. Photoluminescence spectra taken at 5 K from as-grown InAs/GaAs QDs (dashed) and QDs blue-shifted by partial covering (solid). The small peak at 850 nm is emission from the InAs wetting layer.

One of the most studied QD systems is the InGaAs/GaAs heterostructure[17]. In this material combination, the formation of islands reduces the strain energy that accumulates during the epitaxy of InGaAs due to the lattice mismatch with the GaAs matrix. The growing layer of InGaAs clumps into islands after the formation of a thin pseudomorphic layer (wetting layer). As-grown InAs/GaAs QDs have a typical ground state emission wavelength of ~1110 nm. Photoluminescence taken at 5 K from a sample consisting of one layer of as-grown QDs at a density of $\sim 1 \times 10^{10}$ QDs per cm^2 is shown in the dashed line of Fig. 1. The peak at 1110 nm is the ensemble ground state, inhomogenously-broadened due to size fluctuations. The two shorter-wavelength peaks correspond to excited states of the QDs. To shift this emission into a spectral range where our photodetectors have greater efficiency, a specific growth technique has been developed,[18] and it is summarized in Fig. 2. After the clustering of the InAs, QDs are partially covered by a GaAs layer and annealed before completely overgrown. The typical lens shape of the InAs QDs changes to a volcano shape due to the re-melting and desorption of the exposed portion of the InAs islands. The size reduction and Ga-In intermixing blue-shift the ground states of the QDs. Both the growth rate and thickness of the GaAs covering layer determine the amount of energy shift, allowing the QD spectrum to be continuously tuned. We design the QDs in this work to have ground-state emission at ~940 nm. Photoluminescence taken at 5 K from a typical sample of QDs grown

with a 10 Å partial covering layer is shown in the solid line of Fig. 1. The shoulder centered at 940 nm is the ensemble ground state and two excited states are apparent at 920 nm and 905 nm.

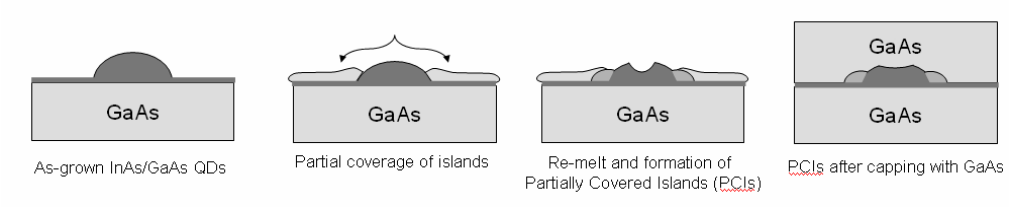

Fig. 2. Schematic of the growth method of InAs/GaAs partially covered islands. A thin layer of GaAs partially covers the InAs islands. Uncovered InAs is then desorbed into the surrounding GaAs, effectively shrinking the QD and blue-shifting its ground-state energy.

3. 2D PHOTONIC CRYSTAL MICROCAVITIES

3.1 Planar photonic crystal fabrication

The cavities described here are created by introducing a defect into a two-dimensional photonic crystal array of air holes in a GaAs substrate. The photonic crystal efficiently confines the light within the defect in the two dimensions that it spans. In order to also confine light in the vertical direction, we suspend the photonic crystal in air, thus creating a slab waveguide 180 nm thick, capable of localizing light by total internal reflection. A simplified schematic of the fabrication process is shown in Fig. 3. First the photonic crystal pattern is defined by electron-beam lithography (EBL) in ZEP 520A electron-beam resist. The pattern is transferred into a GaAs/AlGaAs heterostructure grown by Molecular Beam Epitaxy (MBE) by an anisotropic dry etch. In some cases we first transfer the pattern to an intermediate dielectric mask to improve etch selectivity[3,19]. The slab waveguide is formed by flowing HF acid into the photonic crystal holes and selectively wet-etching the AlGaAs. Scanning electron micrographs (SEMs) of a fully-processed structure are shown in Fig. 3, where only three of ten lattice periods are shown to allow closer inspection of the photonic crystal holes. Details of this fabrication process are provided in [19].

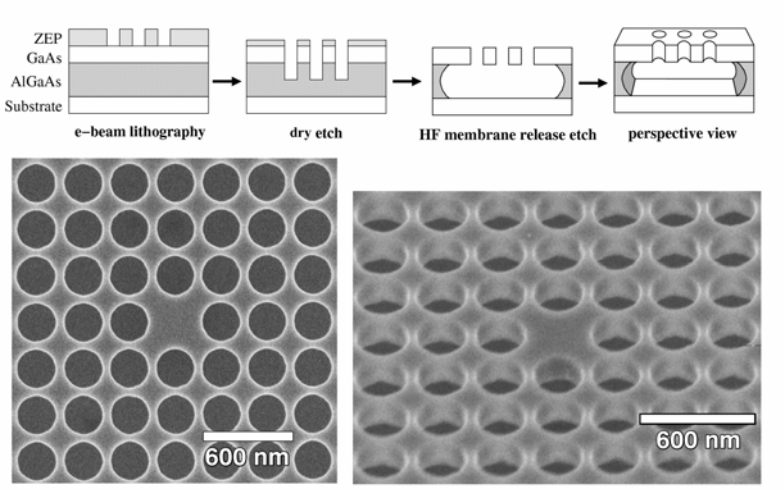

Fig. 3. Schematic of the fabrication process used to create planar photonic crystal cavities and SEMs of a fully-processed device around the defect region. The GaAs slab is 180 nm thick.

3.2 Optical characterization

We determine the resonant wavelength and Q of the defect modes in a low-temperature (5 K) micro-photoluminescence experiment using a high density of QDs embedded in the GaAs slab as an internal light source[3,12]. A typical cavity has five layers of 2×10^{10} QDs per cm^2 incorporated in the GaAs slab. We focus a CW laser through a microscope objective (NA = 0.55) at normal incidence onto a single cavity, exciting carriers in the GaAs. The QDs efficiently capture the carriers and emit photons into the photonic crystal structure. The QD emission is collected through the same objective

and dispersed by a grating monochomator with a resolution of 70 μeV. Due to the high-density of QDs, there is a finite probability of spatial overlap and frequency resonance with a cavity mode. The resonant QDs emit more brightly than off-resonance QDs due to the increased optical density of states in the cavity at the energy of the defect mode. The resulting photoluminescence (PL) spectrum therefore fully characterizes the optical response of the cavity, decorating the modes that the cavity supports over the spectral range illuminated by the QD ensemble. One can extract the Q factors of individual defect modes by measuring the linewidths of the peaks observed in the spectrum. A typical PL spectrum is shown in Fig. 4. Optical emission occurs over a broad wavelength range due to size fluctuations of individual QDs. However, three peaks are apparent in this spectrum, which correspond to the defect modes for this particular cavity. The type, spectral locations, and Q's of these modes are discussed in a later section.

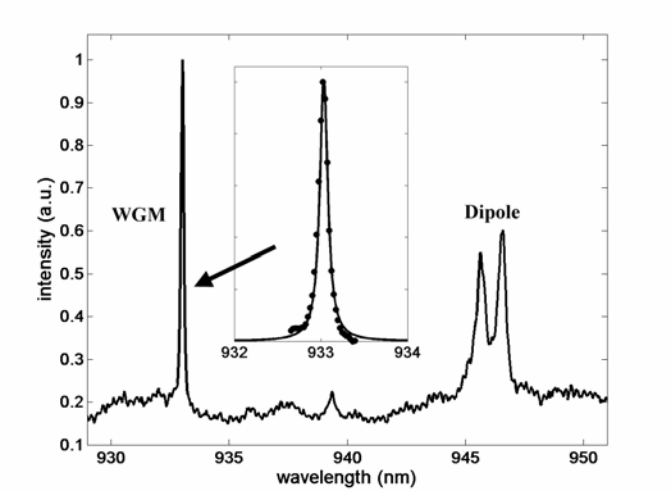

Fig. 4. Photoluminescence spectrum of a high density of QDs in a planar photonic crystal cavity. Emission is observed over a broad wavelength range due to the ensemble QD emission. QDs on resonance with a defect mode emit more brightly, decorating the modal structure of the cavity. In this cavity, three modes are apparent, a high Q whispering-gallery-like mode (WGM) and two dipole modes.

3.3 Choice of lattice symmetry and defect type

Fabrication issues aside, the Q of planar photonic crystal defect modes can change by orders of magnitude depending on the lattice symmetry and defect type. Since all defect modes are well confined in the plane by the photonic crystal, the vast discrepancy in Q is due to certain modes being much more efficiently confined in the vertical direction of these membrane structures. Analyzing defect modes in momentum space reveals that lossy modes contain significant Fourier components with in-plane wave vector amplitudes less than ω_m/c, where ω_m is the angular frequency of the mode. These components can couple to vertical radiative modes and represent the primary source of vertical optical loss. Momentum conservation prevents in-plane Fourier components with wave vector amplitudes larger than ω_m/c from coupling to vertical radiative modes, and these components are totally internally reflected in the semiconductor slab. The lossy components are typically described as being within the light line, where the light line is defined as a circle around the origin of k_x-k_y space with a radius of ω_m/c. A rigorous definition of Q in terms of the integrated wave vector components in the light line is given in [6]. Designing a high-Q cavity therefore amounts to finding defect modes with negligible in-plane Fourier components in the light line. With the fundamental mechanism of vertical loss understood, design rules for constructing high-Q cavities have been developed based on cancellation mechanisms[2] and symmetry analysis[5].

Our initial attempts at characterizing a high Q/V cavity focused on localizing light in defects formed by removing hole(s) from a bulk 2D triangular lattice[3]. The H1 cavity is formed by removing a single hole from the lattice and supports two very small V dipole modes[20]. The amplitude of E_x for one of these modes is shown in Fig. 5 (a). While the mode is confined to a volume approaching the theoretically smallest possible in a dielectric cavity, we measure only modest Q's of ~250, resulting in a Q/V inadequate to observe strong coupling with a single QD. The mode is plotted in momentum space, $|E_x(k_x,k_y)|$, in Fig. 5 (b) revealing the source of the low Q. While the dominant Fourier components are located at the M point, significant components lie within the light line, the solid black circle around the Γ point.

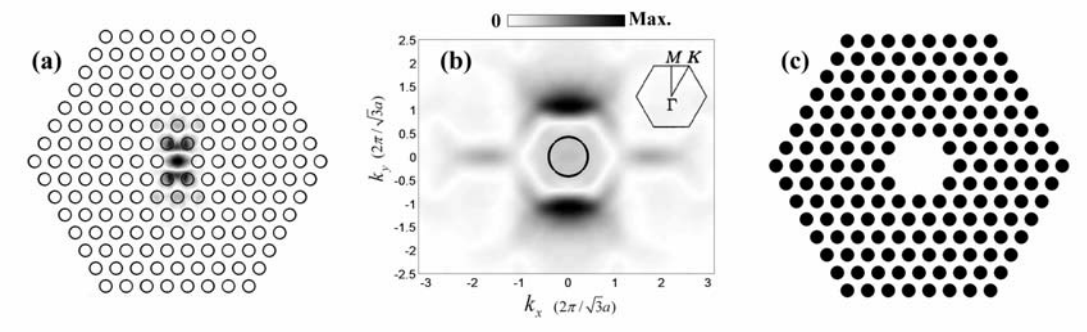

Fig. 5. An H1 cavity is formed in by removing a single hole from a triangular lattice. The structure is depicted with the electric field amplitude $|E_x|$ of one of the dipole modes that it supports in (a). The spatial Fourier transform of this mode $|E_x(k_x,k_y)|$ is shown in (b) and contains significant Fourier components in the light line which degrades its Q. The H2 cavity, formed by removing seven holes, is shown in (c) and supports a doubly-degenerate high Q mode.

We have investigated other defects in the triangular lattice and experimentally discovered a doubly-degenerate, high Q mode in the H2 cavity, which is defined by removing seven holes from the bulk lattice as shown in Fig. 5 (c). While the H2 resonance is larger V than the H1 dipole mode, we demonstrated an increase in Q of over an order of magnitude, as high as 4000, an important step towards realizing a cavity suitable for strong coupling.

More recently, we have characterized the modes of a single-hole defect in a square lattice (S1). This type of cavity is predicted to support two types of modes, a low-Q dipole resonance and a high-Q whispering-gallery-like mode (WGM)[8]. The dipole mode is doubly-degenerate and unimportant for high Q/V applications. However, the electric field intensity distribution of the WGM, as plotted in Fig. 6 (a), shares the same symmetry as the bulk photonic crystal lattice and has a corresponding in-plane electric field distribution that is well balanced in positive and negative energy about each high-symmetry direction of the crystal. This has important implications for the momentum-space representation of the mode, as shown in Fig. 6 (b), where it is apparent that virtually all Fourier components are located outside the light line. The function plotted in Fig. 6 (b) is $|E_x(k_x,k_y)| + |E_y(k_x,k_y)|$ and has dominant Fourier components along most of the entire first Brillouin zone boundary.

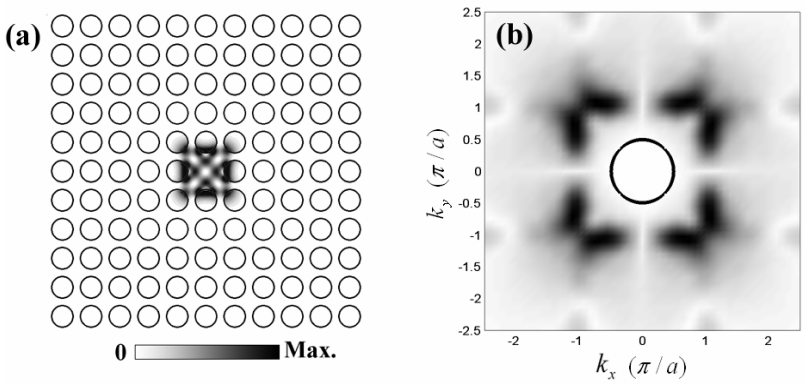

Fig. 6. The S1 cavity is formed by removing a single hole from a bulk square lattice. The cavity supports a high-Q mode with an electric field intensity as shown distributed over space in (a) and over reciprocal space in (b).

Our experimental characterization of this cavity agrees well with theoretical predictions. We observe three distinct modes in the majority of tested devices as exemplified in the spectrum of Fig. 4 for a cavity with a = 295 nm and r/a = 0.38. The lower-Q, closely-spaced resonances are the dipole-x and dipole-y modes with a split degeneracy due to fabrication imperfections. The higher-energy resonance corresponds to the S1 WGM and has a Q as high as 8500, which is determined by fitting the data points of the spectrum to a Lorentzian function as shown in the inset of Fig. 4. By changing the lattice constant a from 280-310 nm and the photonic crystal hole size r/a from 0.36-0.40, we have

demonstrated that the WGM's resonant wavelength can be tuned over the entire spectral range of our QD ensemble, nominally from 870-970 nm as shown in Fig. 1. Due to the single-hole nature of the defect, this cavity has very small V, and thus a Q/V high enough, we estimate, for observing strong coupling with a single QD.

3.4 Sensitivity to fabrication

The choice of proper lattice symmetry and defect type is crucial to achieve cavities with high Q/V; however, imperfections in the fabrication process can also introduce significant sources of optical loss. We have investigated the effect of sidewall inclination on Q by fabricating cavities with different types of dry etches. Our initial process utilized reactive ion etching (RIE) to transfer the photonic crystal pattern from a SiN mask into the (Al) GaAs heterostructure with 10 sccm $SiCl_4$ at 3 mTorr and 100 W. Resulting S1 devices exhibited high Qs of up to 4000 and were characterized over the entire QD ensemble spectrum in [12]. However, a close inspection of the photonic crystal sidewalls revealed substantial deviation from ideality as can be seen in the top SEM in Fig. 7.

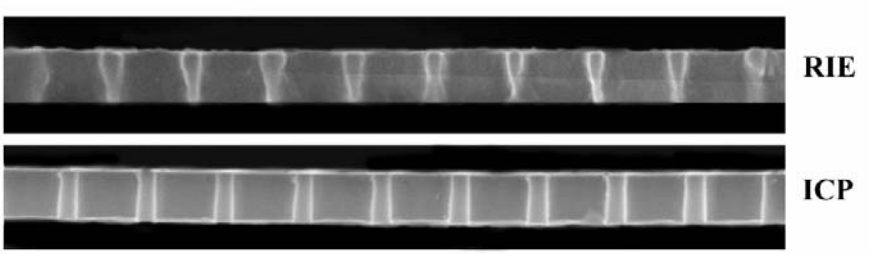

Fig. 7. Cross sections of two photonic crystals, each with a lattice constant of 300 nm. The device in the top panel was etched with an RIE plasma and displays significant variation in r/a throughout the 180 nm GaAs slab. The bottom device was etched in an ICP plasma and has much straighter sidewalls.

In all devices inspected, the RIE sidewalls exhibited significant undercutting resulting in a photonic crystal lattice with r/a ~12% larger at the bottom of the slab than at the top. Since the Q of the WGM is a function of r/a[8], we anticipated that we were not achieving maximum Q.

The optimization of the RIE process was constrained by the necessity to achieve an appreciable etch rate while minimizing sputter-degradation of the mask. Given these constraints, we could not achieve the bias or pressure conditions that might otherwise have produced the most vertical sidewalls. To achieve straighter hole sidewalls, we developed a dry etching process based on an inductively coupled plasma (ICP). The ICP process allows us to generate a dense plasma at relatively low bias conditions which improves the selectivity of our etch enough to obviate the need for an intermediate pattern transfer into SiN. The resulting etch transfers the photonic crystal pattern directly from the ZEP electron-beam resist into the (Al)GaAs heterostructure using a plasma generated from a gas mixture primarily composed of Ar and incorporating both Cl_2 and BCl_3. The optimal conditions for etching through a 180 nm GaAs slab are: 12 sccm Ar, 3 sccm BCl_3, 4 sccm Cl_2, 80 W bias power, 700 W ICP power, and 2.4 mTorr for 135 seconds. Resulting devices have significantly straighter sidewalls than those produced with RIE, as shown in the bottom SEM of Fig. 7. In these devices, r/a varies by only ~2% throughout the GaAs slab. The Q is improved by over a factor of two in the ICP devices, as high as 8500.

Another observed fabrication imperfection in our process is the non-uniformity of photonic crystal hole radius from the center to the edge of a device. The initial pattern is defined by EBL in which every photonic crystal hole is specified to receive the same electron dose. However, due to the backscattering of electrons from the substrate, holes in the center of the device become overexposed compared to those at the device periphery. This effect is commonly referred to as the proximity effect. The result is that r/a decreases from the center to the edge of a device, and this has an important effect on the optical behavior of the cavities.

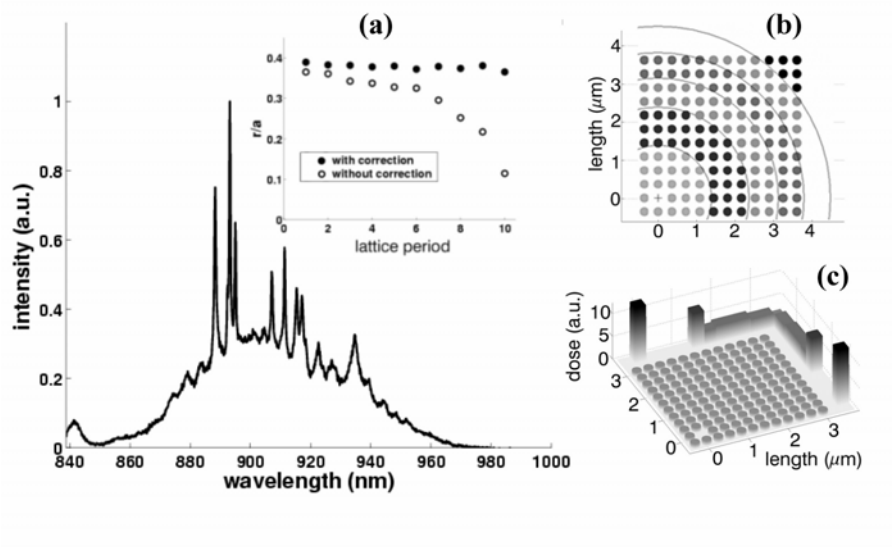

Fig. 8. Photoluminescence spectrum from an S1 device with 6% variation in *r/a* from center to edge. Many closely-spaced, sharp resonances emerge from the broad background QD emission. Hole radius versus lattice period is plotted in (a) for an uncorrected device and one in which the variation in *r/a* was corrected by writing extra high-dose features around the photonic crystal pattern according to (c). Variation in *r/a* may also be corrected by dividing the photonic crystal pattern into areas of increasing electron dose as shown in (b).

A PL spectrum from an S1 device with 6% variation in *r/a* from center to edge is shown in Fig. 8. In contrast to the clear spectrum of Fig. 4, the modal signature of this device is very complex. At least eight different resonances can be identified, and it is impossible to judge from such spectra which peak corresponds to the WGM. We observe these more complex modal signatures in any device with a variation of *r/a* of more than a few percent, and we therefore conclude that the additional peaks correspond to defect modes, not confined to the central defect region, associated with the non-uniform *r/a*. We have investigated two different ways to correct the proximity effect, both based on elevating the dose that the outermost holes receive.

One way to elevate the electron dose of the outermost holes is to deposit large amounts of electron dose around the edge of the device such that the backscattering of these electrons will preferentially overexpose only those holes furthest from the device center. A typical electron dose for one quadrant of an S1 device corrected in this manner is shown in Fig. 8 (c). Each hole receives the same dose which is relatively low compared to extra high-dose features placed outside the cavity. The backscattering from the extra features corrects the variation in *r/a* to under a few percent as shown in the graph of *r/a* versus lattice period in Fig. 8 (a) for two nominally identical devices, one written with the extra features and one without. Details of the design of these extra features are given in [19].

We have demonstrated another way to correct the proximity effect based on direct dose modulation rather than manipulating the backscattered dose distribution across the device. In this method, the photonic crystal holes are separated into regions according to their distance from the center of the device. Each region is then assigned a dose multiplication factor that governs the amount of electron dose the holes in that region receive. A typical division of a device into dose modulation regions is shown in Fig. 8 (b). Resulting devices have negligible variation in *r/a* when the dose multiplication factors are, from the center to the outer corner: 1.00, 1.01, 1.04, 1.09, 1.13, and 1.15. The modal signatures of all devices defined in this way are very clear such as depicted in Fig. 4.

4. POSITIONING OF MICROCAVITIES

A high density of QDs in the GaAs slab is useful for characterizing the optical response of our cavities. However, to build functional devices for quantum information processing, the QD density should be much lower, so that the probability of coupling more than one QD to the defect mode is low. Experiments on a single QD coupled to a cavity mode have been performed in other types of semiconductor cavities such as microdisks[21] and microposts[22]. In these experiments, a single dot was positioned in the cavity by chance. No prior knowledge of the QD position was known

before fabrication of the cavity. There are two reasons why a similar strategy may not be effective in locating a single QD in an S1 device. First, V is much smaller for an S1 cavity than either a micropost or microdisk cavity, significantly lowering the probability of a chance alignment with a single QD. A second important difference between these cavities is that virtually all of the QD material is etched away in micropost and microdisk samples such that any observed QD emission indicates the QD is physically inside the cavity, although possibly not at the antinode of the cavity mode. In contrast, in planar photonic crystal cavities, the QD material is only removed in the photonic crystal holes. Therefore, measured QD luminescence gives relatively little information about the dot's location. The luminescing dot may be located in the bulk photonic crystal or even outside the structure entirely. The combination of these two challenges suggests that developing a means of actively positioning a single QD inside a photonic crystal cavity may be of great importance for efficient construction of quantum information devices.

The active positioning technique proposed here aligns an S1 cavity to a small metal particle on the substrate surface. We are fully aware that this is different from aligning an S1 device to a QD that is buried below the surface (covered by 90 nm of GaAs in our material); however, this is a convenient way to characterize the spatial resolution of our alignment technique. Moreover, we envision ways in which this technique may be extended to align a cavity to QDs located below the surface.

The material used to characterize our active positioning technique is GaAs covered with 65 nm thick Ti alignment marks defined by EBL. Also on the sample are small Ti particles (henceforth "metal dots") created by depositing electron dose at a single point in space at a dose of 30-100 nC/cm in 310 nm of ZEP 520A electron beam resist. After a Ti liftoff, the resulting metal dots are 65 nm high and 35-65 nm in diameter. The first step in our alignment technique is to measure the distance from the origin of a nearby alignment mark to the center of a metal dot. This defines $\vec{r}$ as shown in the left portion of Fig. 9. In this work, we measured $\vec{r}$ using an FEI Sirion SEM.

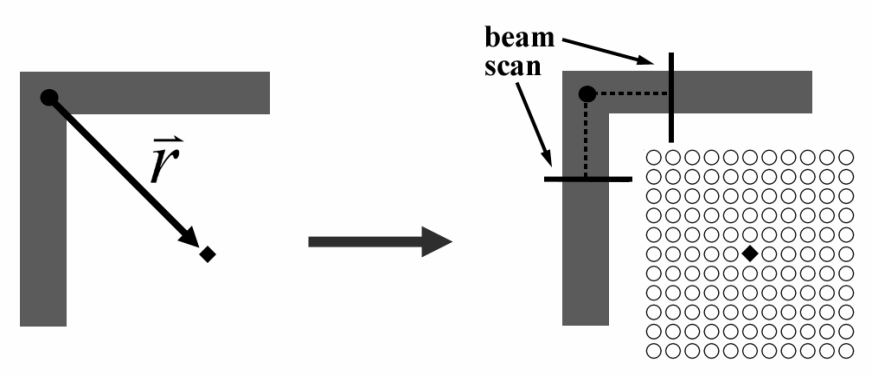

Fig. 9. Positioning an S1 device relative to a small feature on the sample surface is accomplished by first measuring the distance from the feature to the origin of a nearby alignment mark to define $\vec{r}$. The origin is then found by scanning the mark in the EBL system, after which, the S1 pattern is written offset by $\vec{r}$.

The second step in our positioning technique in accomplished by direct-write EBL with a JEOL JBX-5DII (U) system. In this step, the origin of the alignment mark is found by scanning the horizontal and vertical "arms" of the alignment mark to detect the edges of the Ti as depicted by the black lines crossing the alignment mark in the right portion of Fig. 9. These scans detect the widths of the vertical and horizontal arms, from which the origin is derived by extrapolating the center of each arm to a common intersection point as shown by the dashed lines in Fig. 9. With the origin of the alignment mark now defined in the EBL coordinate frame, we then write the S1 pattern offset by $\vec{r}$.

Results of this positioning technique are shown in Fig. 10. The SEM in the left frame was used to determine $\vec{r}$ and shows the vertical and horizontal arms of the alignment mark located near a metal dot indicated by the white arrow. The design of the alignment mark in Fig. 10 is modified to minimize the error in determining the origin. We found that the width of the alignment mark arms increased measurably near the mark origin when the arms were designed to intersect. This is due to the proximity effect, which tends to overexpose the mark where the arms join. By simply not writing the

corner of the mark, we observe a constant width along the entire length of each arm which is necessary for accurate determination of the mark origin in the direct-write EBL. The mark origin was determined by scanning the arms approximately where indicated with the solid white lines in the left portion of Fig. 10 and extrapolating their centers to a common point (dashed lines). An SEM of an S1 device written with an offset of $\vec{r}$ from the origin of a modified alignment mark is shown in the right portion of Fig. 10. In this case, we intended for the metal dot to be centered in the defect and measure an error of ~50 nm. Similar error is measured in the majority of devices. The source of this rather small error is unknown and largely unimportant since this resolution is adequate to position a QD very near the antinode of the defect modes we are investigating.

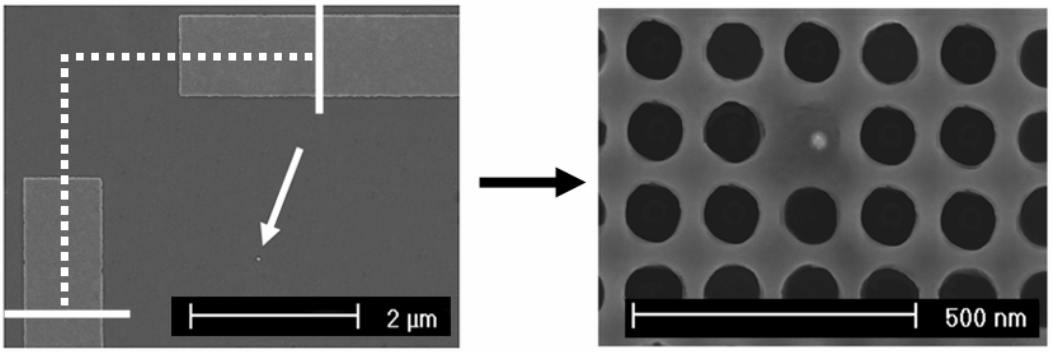

Fig. 10. The left SEM shows the two arms of an alignment mark nearby a small Ti particle on the surface, pointed to by the white arrow. The mark origin was determined by scanning the arms and extrapolating their center to common point, shown schematically by the solid white lines (scan) and dashed lines (extrapolation). The results of our active positioning technique are shown in the right SEM when we intended for the metal dot to be positioned in the center of the defect cavity.

5. CONCLUSION

Defects in planar photonic crystals have the potential to confine light well enough to have a *Q/V* suitable for observing strong coupling with a single QD. The potential for exceptional control of the light comes at the expense of having a severe sensitivity to geometry. Therefore, to realize a high *Q/V* cavity, great care must be taken in the initial choice of symmetry and defect type as well as the fabrication accuracy. We have demonstrated that *Q* can be increased by well over an order of magnitude by either changing the lattice symmetry (H1→ S1) or defect type (H1→ H2). We have also observed the sensitivity of these cavities to fabrication imperfections. It is crucial to minimize the variation in *r/a* across the plane of the photonic crystal to less than a few percent to suppress unwanted, extended defect modes. Two ways of achieving uniform in-plane *r/a* were presented, both based on correcting the proximity effect introduced during the EBL. Variation in *r/a* out of the plane also has important consequences on the optical behavior of these devices, and we showed that by optimizing the dry etching of the holes to decrease the out-of-plane variation in *r/a* from ~12% to ~2%, the *Q* is increased by over a factor of two. The culmination of this work in the analysis and fabrication of planar photonic crystal cavities is a single-hole defect formed in a square lattice that exhibits a *Q* of 8500, quite suitable in our estimates for the observation of strong coupling.

Finally, we have proposed and demonstrated an alignment technique that allows us to position our high *Q/V* cavities to other features on the substrate surface with a resolution of 50 nm. Using a similar technique to align QDs within photonic crystal cavities will have important implications for the efficient construction of quantum information devices. Active positioning is not only desirable because it imparts a full level of control over the alignment process, but it may prove necessary for this class of extremely small *V* devices.

REFERENCES

1. M. Bayer and A. Forchel, "Temperature dependence of the exciton homogeneous linewidth in In/sub 0.60/Ga/sub 0.40/As/GaAs self-assembled quantum dots," *Physical Review B-Condensed Matter* **65**, p. 041308/1 (2002).
2. S. G. Johnson, F. Shanhui, A. Mekis and J. D. Joannopoulos, "Multipole-cancellation mechanism for high-Q cavities in the absence of a complete photonic band gap," *Appl. Phys. Lett.* **78**, p. 3388 (2001).

3. C. Reese, B. Gayral, B. D. Gerardot, A. Imamoglu, P. M. Petroff and E. Hu, "High-Q photonic crystal microcavities fabricated in a thin GaAs membrane," *J. Vac. Sci. Technol. B* **19**, p. 2749 (2001).
4. T. Yoshie, J. Vuckovic, A. Scherer, C. Hao and D. Deppe, "High quality two-dimensional photonic crystal slab cavities," *Appl. Phys. Lett.* **79**, p. 4289 (2001).
5. K. Srinivasan and O. Painter, "Momentum space design of high-Q photonic crystal optical cavities," *Opt. Express* **10**, p. (2002).
6. J. Vuckovic, M. Loncar, H. Mabuchi and A. Scherer, "Optimization of the Q factor in photonic crystal microcavities," *IEEE J. Quantum Electron.* **38**, p. 850 (2002).
7. J. Vuckovic, M. Loncar, H. Mabuchi and A. Scherer, "Design of photonic crystal microcavities for cavity QED," *Phys. Rev. E* **65**, p. 016608/1 (2002).
8. R. Han-Youl, H. Jeong-Ki and L. Yong-Hee, "The smallest possible whispering-gallery-like mode in the square lattice photonic-crystal slab single-defect cavity," *IEEE J. Quantum Electron.* **39**, p. 314 (2003).
9. H. Y. Ryu, M. Notomi and Y. H. Lee, "High-quality-factor and small-mode-volume hexapole modes in photonic-crystal-slab nanocavities," *Appl. Phys. Lett.* **83**, p. 4294 (2003).
10. J. Vuckovic and Y. Yamamoto, "Photonic crystal microcavities for cavity quantum electrodynamics with a single quantum dot," *Appl. Phys. Lett.* **82**, p. 2374 (2003).
11. K. Srinivasan, P. E. Barclay, O. Painter, C. Jianxin, A. Y. Cho and C. Gmachl, "Experimental demonstration of a high quality factor photonic crystal microcavity," *Appl. Phys. Lett.* **83**, p. 1915 (2003).
12. K. Hennessy, C. Reese, A. Badolato, C. F. Wang, A. Imamoglu, P. M. Petroff, E. Hu, G. Jin, S. Shi and D. W. Prather, "Square-lattice photonic crystal microcavities for coupling to single InAs quantum dots," *Appl. Phys. Lett.* **83**, p. 3650 (2003).
13. Y. Akahane, T. Asano, B. S. Song and S. Noda, "High-Q photonic nanocavity in a two-dimensional photonic crystal," *Nature* **425**, p. 944 (2003).
14. D. Bimberg, M. Grundmann and N. N. Ledentsov. *Quantum Dot Heterostructures* (Wiley, New York, 1998).
15. P. M. Petroff, A. Lorke and A. Imamoglu, "Epitaxially self-assembled quantum dots," *Physics Today* **54**, p. 46 (2001).
16. A. Imamoglu, "Are quantum dots useful for quantum computation?," *Physica E* **16**, p. 47 (2003).
17. D. Leonard, M. Krishnamurthy, C. M. Reaves, S. P. Denbaars and P. M. Petroff, "Direct formation of quantum-sized dots from uniform coherent islands of InGaAs on GaAs surfaces," *Appl. Phys. Lett.* **63**, p. 3203 (1993).
18. J. M. Garcia, T. Mankad, P. O. Holtz, P. J. Wellman and P. M. Petroff, "Electronic states tuning of InAs self-assembled quantum dots," *Appl. Phys. Lett.* **72**, p. 3172 (1998).
19. K. Hennessy, C. Reese, A. Badolato, C. F. Wang, A. Imamoglu, P. M. Petroff and E. Hu, "Fabrication of high Q square-lattice photonic crystal microcavities," *J. Vac. Sci. Technol. B* **21**, p. 2918 (2003).
20. O. Painter, T. Vuckovic and A. Scherer, "Defect modes of a two-dimensional photonic crystal in an optically thin dielectric slab," *J. Opt. Soc. Am. B* **16**, p. 275 (1999).
21. P. Michler, A. Kiraz, C. Becher, W. V. Schoenfeld, P. M. Petroff, L. Zhang and A. Imamoglu, "A quantum dot single-photon turnstile device," *Science* **290**, p. 2282 (2000).
22. J. Vuckovic, D. Fattal, C. Santori, G. S. Solomon and Y. Yamamoto, "Enhanced single-photon emission from a quantum dot in a micropost microcavity," *Applied Physics Letters* **82**, p. 3596 (2003).